

# Tetramerization of human guanylate-binding protein 1 is mediated by coiled-coil formation of the C-terminal $\alpha$ -helices

Adrian Syguda<sup>1</sup>, Michael Bauer<sup>2</sup>, Utz Benschaid<sup>1,\*</sup>, Nicole Ostler<sup>2</sup>, Elisabeth Naschberger<sup>2</sup>, Semra Ince<sup>1</sup>, Michael Stürzl<sup>2</sup> and Christian Herrmann<sup>1</sup>

<sup>1</sup> Physical Chemistry I, Ruhr-University Bochum, Bochum, Germany

<sup>2</sup> Division of Molecular and Experimental Surgery, Department of Surgery, University of Erlangen-Nuremberg, Erlangen, Germany

## Keywords

aluminum fluoride; dynamin; protein dimer; protein–protein association; self-assembly

## Correspondence

C. Herrmann, Physical Chemistry I, Ruhr-University Bochum, Universitätsstr. 150, 44780 Bochum, Germany  
Fax: +49 234 3214785  
Tel: +49 234 3224173  
E-mail: chr.herrmann@rub.de

## \*Present address

German Cancer Research Center, Im Neuenheimer Feld 581, 69120 Heidelberg

(Received 15 March 2012, revised 11 May 2012, accepted 11 May 2012)

doi:10.1111/j.1742-4658.2012.08637.x

The human guanylate-binding protein 1 (hGBP1) is a large GTP-binding protein belonging to the dynamin family, a common feature of which is nucleotide-dependent assembly to homotypic oligomers. Assembly leads to stimulation of GTPase activity, which, in the case of dynamin, is responsible for scission of vesicles from membranes. By yeast two-hybrid and biochemical experiments we addressed intermolecular interactions between all subdomains of hGBP1 and identified the C-terminal subdomain,  $\alpha$ 12/13, as a new interaction site for self-assembly.  $\alpha$ 12/13 represents a stable subdomain of hGBP1, as shown by CD spectroscopy. In addition to contacts between GTPase domains leading to dimer formation, the interaction between two  $\alpha$ 12/13 subdomains, in the course of GTP hydrolysis, results in tetramer formation of the protein. With the help of CD spectroscopy we showed coiled-coil formation of two  $\alpha$ 12/13 subdomains and concentration-dependent measurements allow estimating a value for the dissociation constant of 7.3  $\mu$ M. We suggest GTP hydrolysis-driven release of the  $\alpha$ 12/13 subdomain, making it available for coiled-coil formation. Furthermore, we can demonstrate the biological relevance of hGBP1 tetramer formation in living cells by chemical cross-link experiments.

## Structured digital abstract

- [hGBP1](#) and [hGBP1](#) bind by [cross-linking study](#) (View interaction)
- [hGBP1](#) and [hGBP1](#) bind by [molecular sieving](#) (View Interaction: [1](#), [2](#))
- [hGBP1](#) physically interacts with [hGBP1](#) by [two hybrid](#) (View Interaction: [1](#), [2](#), [3](#))

## Introduction

The human guanylate-binding protein 1 (hGBP1) belongs to the dynamin superfamily of large GTPases. A major cellular function of dynamin is scission of membrane vesicles as a result of its properties as a mechanochemical enzyme [1]. Nucleotide binding and

hydrolysis by the GTPase domain induces a structural change of the helical part of the protein, leading to major rearrangements of the dynamin oligomer [2]. In contrast to dynamin, the cellular function of the human guanylate-binding proteins belonging to the

## Abbreviations

DMS, dimethyl sulfoxide; EDC, 1-Ethyl-3-(3-dimethylaminopropyl)carbodiimide hydrochloride; FL-hGBP1, full-length human guanylate-binding protein 1; GAPDH, glyceraldehyde-3-phosphate dehydrogenase; GDP, guanosine diphosphate; GMP, guanosine monophosphate; GppNHp, a nonhydrolysable GTP analog; GST, glutathione S-transferase; GTP, guanosine triphosphate; hGBP1, human guanylate-binding protein 1; HUVECs, human umbilical vein endothelial cells; IFN- $\gamma$ , interferon- $\gamma$ ; LG, large globular; MMP-1, matrix metalloproteinase-1; NHS, N-hydroxysulfosuccinimide.

same superfamily of large GTPases is not completely understood. Therefore, in recent years several publications have focused on elucidating the biological function of hGBP1 and, so far, it has been found to be linked to various diseases. It could be demonstrated that hGBP1 mediates an antiviral effect against vesicular stomatitis virus, encephalomyocarditis virus and hepatitis C virus and, additionally, it is linked to bacterial diseases such as bacterial meningitis and *Chlamydia trachomatis* [3–6]. Moreover, hGBP1 has been shown to mediate the anti-angiogenic effects of inflammatory cytokines in cultured endothelial cells *in vitro* [7,8] and in tumor vessel endothelial cells of colorectal carcinoma patients *in vivo* [9]. Furthermore, it has been demonstrated that overexpression of hGBP1 is associated with different types of tumors, such as glioblastoma [10], oral cancer [11] and mammary cancer [12]. In two other studies, overexpression of GBP1 was observed to be associated with paclitaxel resistance in ovarian cancer cells and with docetaxel resistance in prostate cancer cells [13,14].

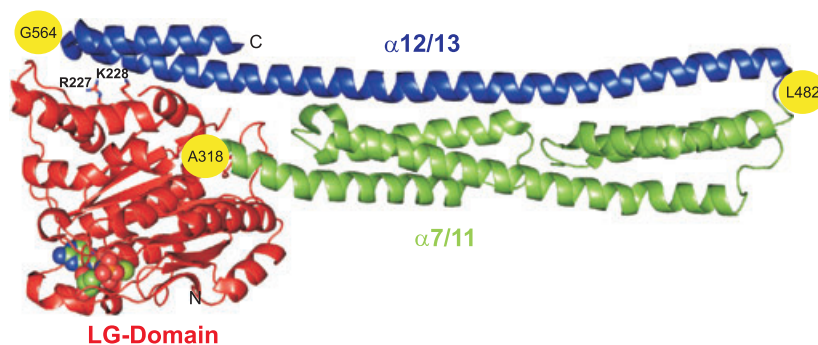
Biochemically, hGBP1 shows nucleotide-dependent oligomerization and a high intrinsic GTPase activity, both of which are characteristic properties of members of the dynamin superfamily. It could be further shown that the GTPase activity of hGBP1 is strongly increased by dimer and tetramer formation, which reflects the importance of self-association, similarly to dynamin [15,16]. The most distinguishing feature of hGBP1 is the catalysis of guanosine triphosphate (GTP) hydrolysis, leading to the formation of guanosine monophosphate (GMP) by two successive phosphate-cleavage steps [15,17].

hGBP1 is composed of two domains: a large globular (LG) domain at the N-terminus that harbors the nucleotide-binding site; and a C-terminal domain with an elongate shape that consists only of  $\alpha$ -helices and connecting loops (Fig. 1) [18]. Various crystal structures of the LG domain of hGBP1 bound to different nucleotides have been solved [19]. The mechanism of

hGBP1-catalyzed nucleotide hydrolysis could be elucidated on the basis of these crystal structures and on biochemical experiments [20,21]. In addition to dimer formation by the LG domain, full-length hGBP1 was found to form larger oligomers, most likely homo tetramers, in the course of GTP hydrolysis or in the presence of guanosine diphosphate (GDP) and aluminum fluoride [22]. hGBP1 in complex with GDP.AIF<sub>x</sub> with the planar configuration of the  $\gamma$ -phosphate represents a mimic of the transition state of GTP hydrolysis, which is reported for many other GTPases. While it is well understood how dimer formation through the LG domains accelerates GTP hydrolysis, the structure and function of higher oligomers of hGBP1 are not known. Until now it was not possible to solve the crystal structure of full-length hGBP1 in complex with GDP.AIF<sub>x</sub> to identify the contact areas of hGBP1 that are responsible for tetramer formation. However, our recent findings suggest a structural change within the helical part of hGBP1 in the course of GTP hydrolysis, which may uncover a second interaction site that mediates tetramer formation [23].

Reflecting the biological function of hGBP1, it is worthy of note that the helical domain plays an important role. In certain cell systems the C-terminal helical domain, but not the LG domain, induces expression of matrix metalloproteinase-1 (MMP-1) [10], whereas the GTPase activity of GBP-1 is required to induce expression of MMP-1 in other cell types [7] and, furthermore, the helical domain alone could induce invasiveness of glioblastoma multiforme [10]. Another publication shows that the helical domain alone is sufficient to inhibit endothelial cell proliferation [24]. Dimerization of GBP-1, as well as heterodimerization of different members of the GBP family, has recently been demonstrated in living cells [25]. Therefore, in this work we set out to elucidate the role of the helical domain in the interaction between hGBP1 molecules. We employed yeast two-hybrid analysis, chemical cross-linking and CD spectroscopy to define the

**Fig. 1.** Structure of hGBP1. Crystal structure of hGBP1 in complex with GppNHp (spheres) presented as a ribbon (PDB: 1F5N). The N-terminal large GTPase domain (LG domain) is coloured in red. The elongate, purely  $\alpha$ -helical, domain is divided into two subdomains:  $\alpha$ 7/11 (green) and the C-terminal helices  $\alpha$ 12/13 (blue). The yellow dots indicate the domain boundaries referred to in the text.



contribution of individual hGBP1 domains in the formation of homomeric hGBP1 complexes and to establish a model for the hGBP1 tetramer.

## Results and Discussion

hGBP1 is a large GTP-binding protein that can be subdivided into a compact LG domain and an elongated, purely helical, domain at the C-terminus. The LG domain (Fig. 1, red) contains the conserved sequence motifs indicative for guanine nucleotide binding. The LG domain on its own is able to form homodimers in a nucleotide-dependent manner but no larger complexes [16]. Here we sought to characterize the interactions between hGBP1 molecules in the fully assembled, tetrameric state. Therefore, DNA constructs were generated that encoded the following hGBP1 subdomains: (a) the LG domain (Fig. 1, red), (b) the full helical domain (hereafter termed  $\alpha 7/13$ ) consisting of residues 318–592 (Fig. 1, green and blue) and the helical subdomains containing (c) residues 318–482 (hereafter termed  $\alpha 7/11$ , Fig. 1, green), (d) residues 483–592 (hereafter termed  $\alpha 12/13$ , Fig. 1, blue) and (e) residues 1–481 (Fig. 1, red and green) (which comprised the full protein except for  $\alpha 12/13$ ).

### Defining the interacting domains of hGBP1

In a first step, the DNA constructs encoding the proteins mentioned above and full-length hGBP1 (FL-hGBP1) were cloned into the yeast two-hybrid vectors, pGBKT7 and pGADT7 [26]. The yeast two-hybrid method offers the advantage that homotypic as well as heterotypic interactions can be analyzed. Typical results of screening hGBP1 interactions by growth on interaction test plates (media lacking tryptophan, leucine, histidine and adenine, QDO) are shown in Fig. S1, in addition to controls of successful cotransfection of pGBKT7 and pGADT7 by growth on diploid growth control plates (media lacking tryptophan and leucine, DDO). The results of such yeast two-hybrid experiments are summarized in Table 1 and show that FL-hGBP1 can interact with FL-hGBP1 and with the LG domain, as expected according to our previous biochemical and structural data [16,20]. In addition, we observed an interaction between FL-hGBP1 and the helical domain ( $\alpha 7/13$ ). In contrast, there was no interaction reported in the yeast two-hybrid assay between FL-hGBP1 and the subdomain  $\alpha 7/11$  but an interaction was observed between FL-hGBP1 and the C-terminal part ( $\alpha 12/13$ ).

**Table 1.** Interactions between hGBP1 domains identified by yeast two-hybrid assays. FL-hGBP and the C-terminal helices  $\alpha 12/13$ , fused to the GAL4-activation domain using vector pGADT7, were each tested for interaction with the listed hGBP1 domains fused to the DNA-binding domain using vector pGBKT7. +, growth on the interaction test plates; –, no growth, on the interaction test plates.

Interaction with FL-hGBP		Interaction with $\alpha 12/13$	
FL-hGBP	+	FL-hGBP	+
LG-domain	+	LG-domain	–
$\alpha 7/13$	+	$\alpha 7/13$	+
$\alpha 7/11$	–	$\alpha 7/11$	–
$\alpha 12/13$	+	$\alpha 12/13$	+

The second interaction domain of hGBP1, mapped to helices  $\alpha 12/13$ , was tested for interaction with hGBP1 domains in a second set of yeast two-hybrid experiments (Table 1).  $\alpha 12/13$  was found to interact with FL-hGBP1, but not with the LG domain. Furthermore, an interaction was reported between  $\alpha 12/13$  and  $\alpha 7/13$  but not between  $\alpha 12/13$  and  $\alpha 7/11$ , lacking the two helices  $\alpha 12$  and  $\alpha 13$ . Finally, we observed homotypic interaction of  $\alpha 12/13$ . Additional yeast two-hybrid experiments addressing the homotypic interactions of  $\alpha 7/13$  and  $\alpha 7/11$ , respectively, yielded a positive result for  $\alpha 7/13$  and no interaction between two  $\alpha 7/11$  molecules (data not included in Table 1). Taken together, our two-hybrid results identify the C-terminal subdomain  $\alpha 12/13$  as a new interaction site for self-assembly of hGBP1. Thereby, the subdomain  $\alpha 12/13$  seems to interact with  $\alpha 12/13$  of another molecule which, in addition to the interactions of the LG domain, would lead to tetramer formation.

In order to confirm the homotypic interaction between  $\alpha 12/13$  fragments, as indicated by yeast two-hybrid analysis, we subjected the purified protein to chemical cross-link experiments. 1-Ethyl-3-[3-dimethylaminopropyl]carbodiimide hydrochloride (EDC/NHS) and dimethyl suberimidate (DMS) were used as cross-linking agents and the reaction products were analyzed by SDS/PAGE. The time course of the reaction of  $\alpha 12/13$  with EDC is documented in Fig. 2A. Remarkably, even after a very long incubation (3 h), a dimer was observed, but no larger products. Reaction with DMS, an imidoester cross-linker with an 11-Å spacer, showed the same result for the interaction of  $\alpha 12/13$  (Fig. 2B). The chemical cross-linking of the  $\alpha 7/13$  dimer is less efficient, suggesting that the interaction has lower affinity. More intriguingly, the  $\alpha 7/11$  fragment does not reveal any dimer formation in this cross-linking assay, either using EDC/NHS (data not shown) or using DMS (Fig. 2B). All these observations

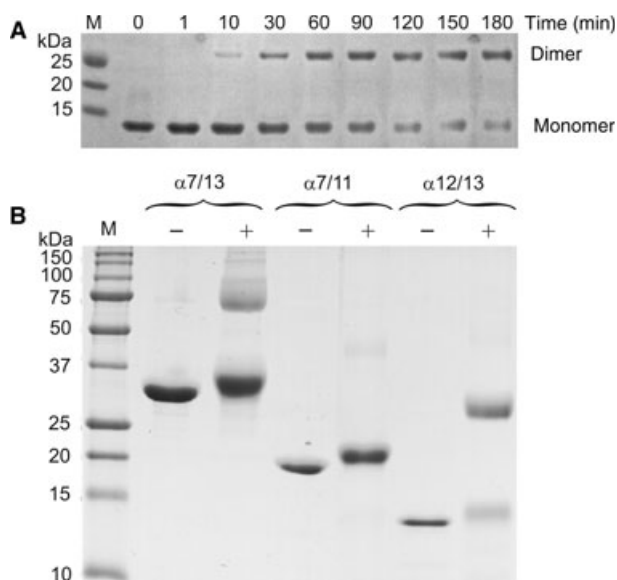


**Fig. 2.** Cross-linking of different helical hGBP1 fragments. (A) Progress of the cross-linking reaction of 30 μM α12/13 with 10 mM EDC and 20 mM NHS at the indicated time-points. After 1 h of incubation, half of the protein is found to be covalently linked, whereas more than 80% dimer product is observed after 3 h. (B) Cross-linking reaction of different constructs of the helical domain with 25 mM DMS. +, presence of cross-linker; -, absence of cross-linker.

are in full agreement with the conclusions from the yeast two-hybrid experiments and support the hypothesis that α12/13 plays a role in the formation of hGBP1 tetramers.

### α12/13 is essential for hGBP1 tetramer formation

Nucleotide-dependent oligomerization of hGBP1 has already been documented [16,20]. In the absence of nucleotides, hGBP1 is a monomer, whereas after binding of a non-hydrolysable GTP analog (GppNHp), a protein dimer is observed using FL-hGBP as well as the LG domain of hGBP1. After addition of GTP or in the presence of GDP and aluminum fluoride, FL-hGBP forms a tetramer, whereas the protein fragment comprising the LG domain forms a dimer. So far it is not known how the tetramer is established in the course of GTP hydrolysis or when bound to GDP and aluminum fluoride. The observations presented here suggest a role for the helical part in tetramer formation.

Our findings on the potency of α12/13 to form a homotypic complex prompted us to address the role of α12/13 in nucleotide-dependent oligomerization of FL-hGBP in more detail. To confirm our hypothesis that α12/13 interaction is responsible for tetramer

formation of hGBP1, we generated an hGBP1-deletion mutant lacking α12/13 (red and green in Fig. 1, comprising residues 1–481). This mutant shows a strong impact on the nucleotide hydrolysis, as reported earlier. The GTPase activity shows a catalytic constant of 60 min<sup>-1</sup>, which is nearly three times larger than that of the wild-type protein (22.8 min<sup>-1</sup>) [33]. After calibration with standard proteins, size-exclusion chromatography experiments showed nucleotide-free FL-hGBP protein as a monomer. Dimer formation was observed after the addition of GppNHp, whereas in the presence of GDP and aluminum fluoride, FL-hGBP eluted as a protein tetramer (Fig. 3A), as shown previously [16,20]. Deletion of C-terminal helices α12/13 showed an interesting change in this picture (Fig. 3B). While the protein was still a monomer in the nucleotide-free form (Fig. 3B, solid line) and a dimer in the presence of GppNHp (Fig. 3B, dashed line), only dimer formation was observed in complex with GDP.AIF<sub>x</sub> (Fig. 3B, dotted line). This can be explained by dimer formation through the LG domain and the necessity of the C-terminal subdomain α12/13 for the establishment of a tetramer.

### Prediction of coiled-coil regions in hGBP1

Because of the presence of α-helical content of the C-terminus of hGBP1, we inspected the sequence using the COILS program, which predicts α-helical coiled-coil domains in proteins [27]. This prediction shows a high probability (> 0.8) for residues 482–563 (α12) to form coiled-coils under stringent conditions (scanning windows of 28 residues) by identification of the characteristic heptad repeats (Fig. 4A). This region is composed of 11 heptad repeats that have a pattern characteristic for α-helical coiled-coil motifs. In Fig. 4C, the residues of this region are listed according to the heptad repeats pattern. In these heptad repeats, the indicated positions **a** and **d** represent predominantly hydrophobic residues (Fig. 4C, columns in light grey), positions **e** and **g** show mainly charged or polar residues (Fig. 4C, columns in dark grey) and positions **b**, **c** and **f** are not so uniformly specified. This pattern is interrupted three times, possibly in order to prevent overwinding of the supercoil [28]. For helix α13 this prediction shows a probability of around 0.5 for coiled-coil formation (not listed in Fig. 4C).

Looking at the surface electrostatic potential of helix α12, a pattern of positively and negatively charged residues is evident (Fig. 4B). There are 19 negatively charged Asp and Glu residues within this 85-residue helix, together with 16 positively charged Arg and Lys

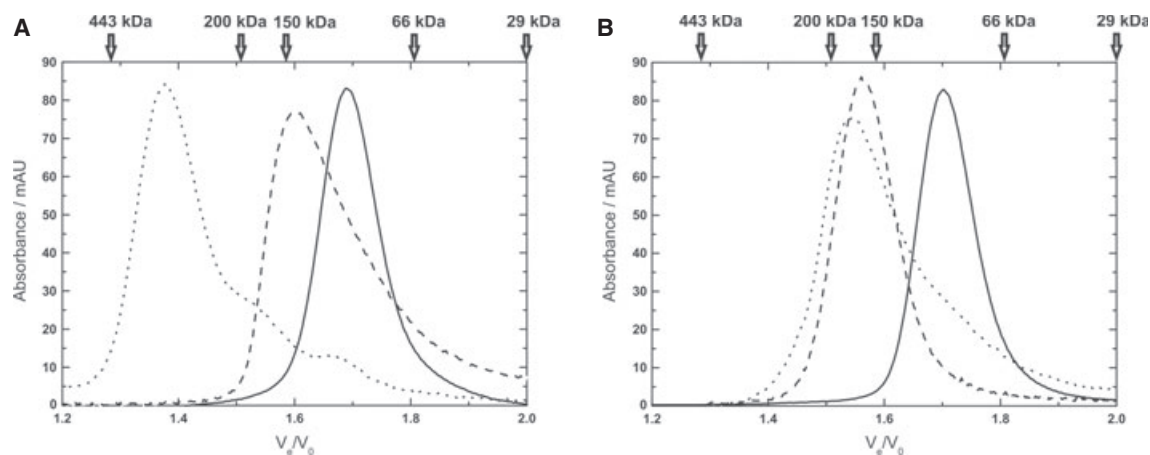


**Fig. 3.** Size-exclusion chromatography of hGBP1 in the presence of GppNHp (dashed line), GDP.AIFx (dotted line), and in the absence of any nucleotide (continuous line), respectively. The absorbance at 280 nm is plotted against the elution volume ( $V_e$ ) of the protein divided by the void volume ( $V_0$ ) of the column. (A) FL-hGBP1. (B) Deletion mutant hGBP1 (1–481) lacking  $\alpha$ 12/13.

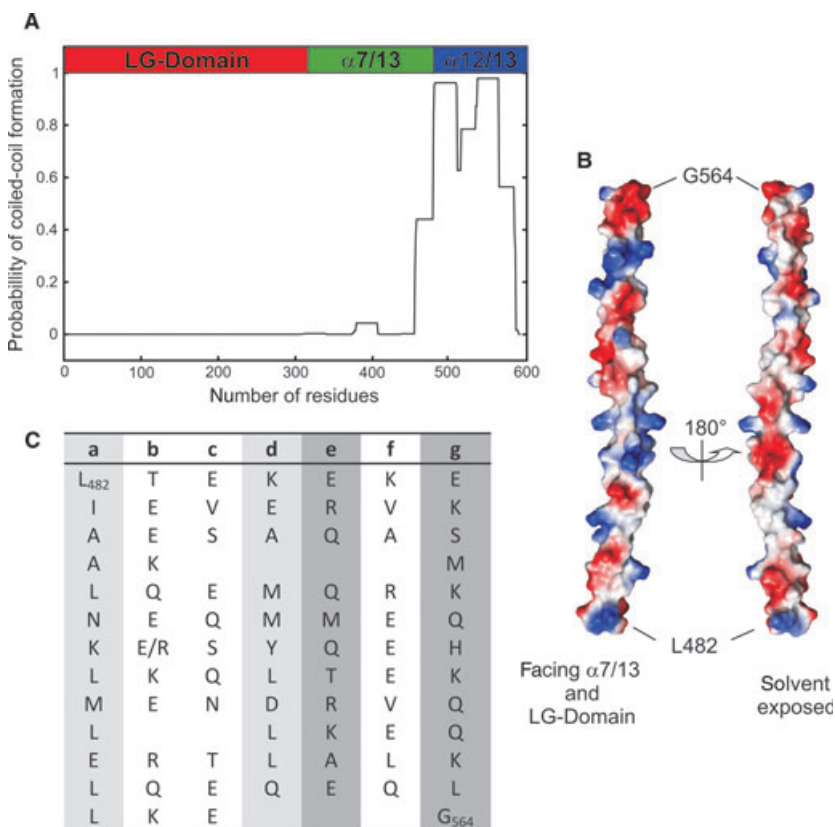


**Fig. 4.** COILS analysis of hGBP1. (A) Plot showing the highest probability of coiled-coil formation at the C-terminal helices  $\alpha$ 12/13, as predicted by COILS, using the most stringent criteria (scanning windows of 28 residues). (B) Distribution of charged residues of hGBP1  $\alpha$ 12 (residues 482–564). The left-hand structure shows the side buried in the full-length protein. The residues on the right-hand structure are exposed to the solvent, also in the full-length protein. Negatively charged residues are red and positively charged residues are blue. (C) Amino-acid sequence of the coiled motif of hGBP1 residues 482–564, according to the COILS prediction. The letters a–g at the top of the columns designate the positions within the heptads.

residues. Most of the charged residues are not solvent exposed, but are buried in the full-length protein. The X-ray structure revealed only weak interactions between  $\alpha$ 12/13 and the middle domain,  $\alpha$ 7/11, and there were no specific contacts within the usual distance of salt bridges and H-bonds, as presented pre-

viously [18]. The polar and charged residues buried between  $\alpha$ 12/13 and  $\alpha$ 7/11 subdomains could be important for solubilizing the residues exposed after separation of the two subdomains, as discussed later. In addition, they may serve for coiled-coil formation, as suggested in the next section.

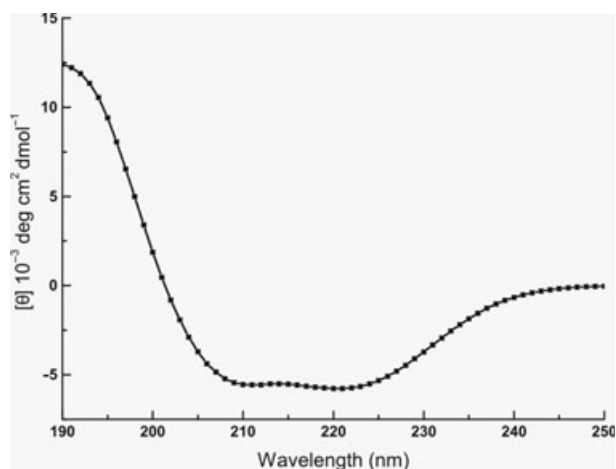


**Fig. 5.** CD-spectrum of FL-hGBP1. The spectrum was recorded at 10  $\mu\text{M}$  protein concentration at 25  $^{\circ}\text{C}$  and normalized according to the cell path length, protein concentration and number of amino acid residues.

**Table 2.** Secondary-structure determination of hGBP1 fragments using CD. The percentage of secondary structure elements was calculated from a fit to the CD spectra using the DICHROWEB server [29]. The numbers represent percentage (respective values observed in the crystal structure). PDB: 1DG3.

	Helical structure	$\beta$ -sheet structure	Turns	Unstructured regions
FL-hGBP	66 (57.4)	8 (9.5)	7 (4.5)	19 (28.5)
LG domain	42 (36.1)	13 (17.0)	15 (5.5)	30 (41.3)
$\alpha$ 7/13	77 (84.3)	7 (0)	6 (12.0)	10 (3.7)
$\alpha$ 7/11	84 (83.5)	5 (0)	5 (2.5)	6 (14.0)
$\alpha$ 12/13	82 (86.0)	3 (0)	5 (5.0)	10 (9.0)

## Interactions between hGBP1 domains

For biochemical characterization of the coiled-coil interactions between the hGBP1 fragments defined above, they were synthesized in bacteria and purified by chromatography. CD spectroscopy is a highly sensitive method for reporting  $\alpha$ -helical structures and especially coiled-coil formation. A typical CD spectrum is shown for FL-hGBP1 in Fig. 5, exhibiting two minima at 208 and 222 nm and a maximum near 190 nm, respectively. This spectrum is characteristic for proteins with mainly  $\alpha$ -helical content and is in agreement with the crystal structure of hGBP1.

The structural integrity of all proteins used in this study was tested by probing their secondary structure using CD spectroscopy. After analysis, the proportion of  $\alpha$ -helices,  $\beta$ -sheets, turns and unstructured regions were compared with the known crystal structure of hGBP1, as shown in Table 2. We found good agreement between the results of the analyses of our CD spectra and the crystal structure for all hGBP1 fragments. Thus, the hGBP1 protein fragments adopt a native-like structure, as observed in the crystal structure of FL-hGBP.

Next, we studied the protein concentration-dependence of the CD spectrum in order to address homotypic interactions of the protein. By using various deletion and point mutants of hGBP1, a clear effect of the protein concentration on the CD spectrum was observed. Figure 6A shows the collected spectra for the isolated helices  $\alpha$ 12/13 at increasing concentrations, scaled as the mean residue ellipticity  $[\theta]$  according to Eqn (1), taking into account the cell path-length ( $l$ ), concentration ( $c$ ) and the mean residue weight [ $MRW = M/(N-1)$ , where  $M$  is the molar mass of the polypeptide chain and  $N$  is the number of residues].

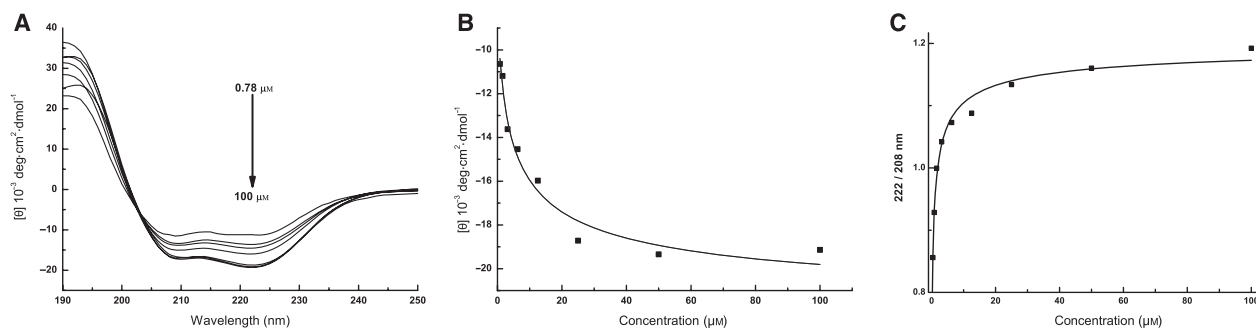


**Fig. 6.** Change of molar ellipticity as a function of protein concentration. (A) CD spectra of hGBP1  $\alpha$ 12/13 at various concentrations. CD measurements were recorded in a Jasco J-810 spectropolarimeter using a different path length cell. Each spectrum was accumulated at least 10 times at 25  $^{\circ}\text{C}$ . (B) Ellipticity at 222 nm as a function of protein concentration. (C) Ratio of the ellipticity of 222 and 208 nm as a function of protein concentration.

$$[\theta] = \frac{\theta * MRW}{c * l} \quad (1)$$

By increasing the concentration, the ellipticity shifts to more negative values, implicating formation of coiled-coils [30,31]. Assuming that this shift is caused by a monomer-to-dimer transition by forming a coiled-coil, we plot the mean residue ellipticity at 222 nm against the concentration, leading to a decrease. Equation (2), representing the ellipticity change according to a monomer/dimer equilibrium, is fitted to the data, providing the equilibrium dissociation constant ( $K_d$ ) of the  $\alpha 12/13$  dimer (7.3  $\mu\text{M}$ ) (Fig. 6B). Further evidence supporting the coiled-coil formation of  $\alpha 12/13$  is given by the ratio of ellipticity values at 222 and 208 nm. The change at 208 nm is caused by the conversion of a rigid single-stranded  $\alpha$ -helix to an  $\alpha$ -helical coiled-coil structure, as the  $\pi$ - $\pi^*$  excitation band polarizes parallel to the helix axis. The increase of the ratio value from 0.85 at 0.78  $\mu\text{M}$   $\alpha 12/13$  to 1.17 at 100  $\mu\text{M}$   $\alpha 12/13$  is shown in Fig. 6C. By fitting Eqn (2) to the obtained set of ratios, an equilibrium dissociation constant of about 1  $\mu\text{M}$  was obtained (Fig. 6C). In Eqn (2),  $x$  represents the protein concentration,  $y$  the ellipticity and ratio value, respectively, and  $max$  and  $min$  the maximal and minimal ellipticity and ratio values, respectively.

$$y = Y_{\min} + \frac{(Y_{\max} - Y_{\min})}{4 \times x + K_d - \sqrt{K_d^2 + 8 \times x \times K_d}} \quad (2)$$

The ratio of  $[\theta]_{222}/[\theta]_{208}$  can be taken as a measure of  $\alpha$ -helicity, in particular the  $\alpha$ -helical supercoiling associated with coiled-coil formation. Ratios approaching 1.0 or higher are reported to be indicative of fully folded coiled-coils. A ratio of 0.85 is indicative for single stranded  $\alpha$ -helices [31,32].

In our previous study on hGBP1 interactions, we identified residues in the contact area between the LG domain and  $\alpha 12/13$  that were responsible for the adherence between these two domains. We showed that the double mutant R227E/K228E leads to a change of the hGBP1 structure, presumably as a result of some kind of detachment of  $\alpha 12/13$  from the rest of the protein. In this mutant the salt bridge network connecting helix  $\alpha 4'$  of the LG domain with the C-terminal part of  $\alpha 12/13$  is destroyed, releasing the contact. Previously buried parts of  $\alpha 12/13$  may become available for interaction. This mutant was shown to form a dimer in the absence of nucleotide, and the GTPase activity was slightly increased, to

36.2  $\text{min}^{-1}$ , at 25 °C compared with that of the wild-type protein (22.8  $\text{min}^{-1}$ ) [33]. We used this hGBP1 mutant in the present study in order to address the behavior of  $\alpha 12/13$  in the context of the FL-hGBP1. As with  $\alpha 12/13$  alone, we observed a concentration dependence of the CD signal for this mutant. Upon increasing the concentration of this double mutant, the monomer-to-dimer equilibrium was shifted toward formation of coiled-coil dimer, indicated by more negative ellipticity values at 208 and 222 nm. At protein concentrations larger than 2  $\mu\text{M}$ , the ellipticity no longer showed much change with increasing protein concentration, indicating a smaller  $K_d$  value of the double-mutant dimer compared with the  $\alpha 12/13$  dimer. The fit to the data according to Eqn (2) is shown in Fig. 7B, yielding a dissociation equilibrium constant of 0.7  $\mu\text{M}$  for the double mutant and thereby indicating a 10-fold higher affinity compared with the isolated  $\alpha 12/13$  dimer.

Using the isolated helices  $\alpha 7/13$ , a concentration dependency of the CD spectra is not observed in the range between 1 and 40  $\mu\text{M}$  (Fig. S2A). This can be explained by no or only weak interaction between two  $\alpha 7/13$  molecules. This observation is not in disagreement with the chemical cross-linking results obtained for  $\alpha 7/13$  shown in Fig. 2. Cross-linking between  $\alpha 7/13$  molecules, leading to covalent dimers, was found to be less efficient than crosslinking between  $\alpha 12/13$  molecules, suggesting lower affinity between  $\alpha 7/13$  molecules. Likewise, differentiation between weak and strong interactions in quantitative terms is also difficult in the yeast two-hybrid assay, where we reported  $\alpha 7/13$  interaction as well. Unfortunately, it was not possible to collect CD spectra at higher protein concentrations as the absorption becomes too high beyond 40  $\mu\text{M}$ . Looking at the CD spectra of wild-type FL-hGBP, no change in the ellipticity with increasing protein concentrations is observed either (Fig. S2B). This is expected as  $\alpha 12/13$  is tightly attached to the rest of the protein through the salt-bridge contact mentioned above. Only binding of GDP.AIF<sub>x</sub> or GTP hydrolysis may lead to distortion of the salt bridge contact, leading to release of  $\alpha 12/13$  and subsequent interaction between two  $\alpha 12/13$  domains. Together with the contact between two LG domains this may result in the formation of a tetramer (Fig. 8).

### Tetramer formation of hGBP1 in living cells

Finally, we were interested in whether our biochemical results are relevant for the hGBP1 protein in a living cell. To this end we carried out formaldehyde cross-linking of interferon- $\gamma$  (IFN- $\gamma$ )-stimulated human umbilical vein endothelial cells (HUVECs) expressing

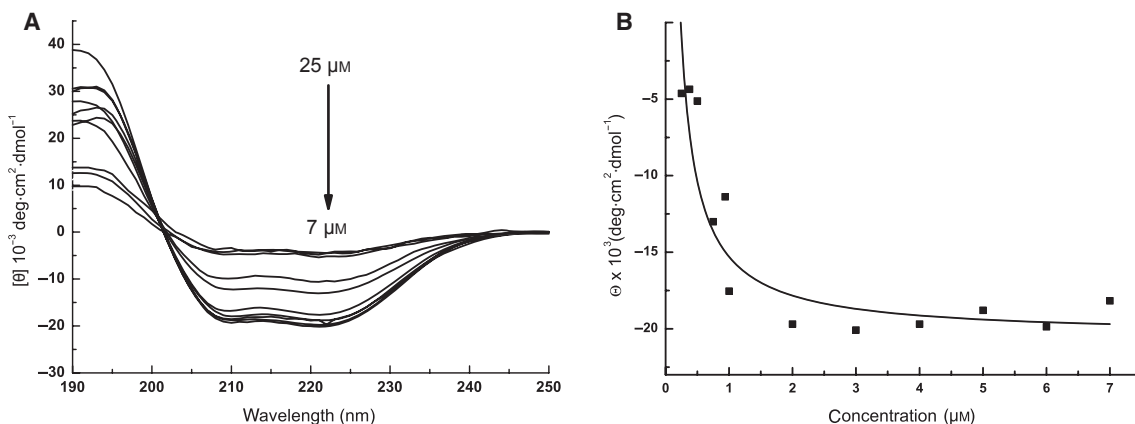


**Fig. 7.** Change of the molar ellipticity as a function of protein concentration. (A) CD spectra of different concentrations of the charge reverse mutant hGBP1, R227E/K228E. CD measurements were recorded using a Jasco J-810 spectropolarimeter using a different path length cell. Each spectrum was accumulated at least 10 times at 25 °C. (B) Ellipticity at 222 nm as a function of protein concentration is shown.

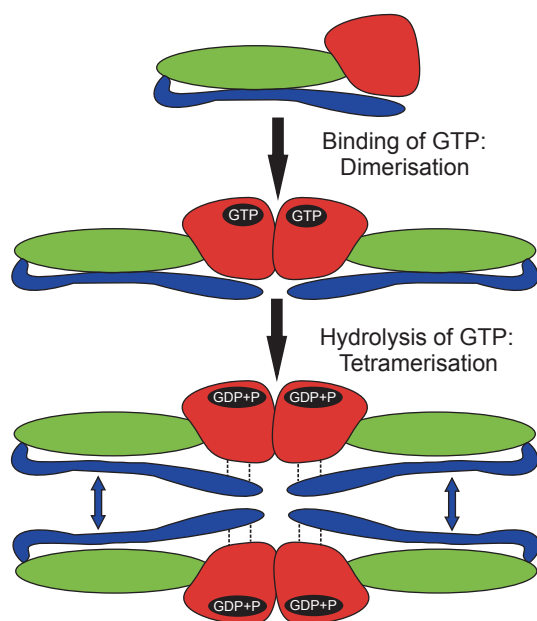


**Fig. 8.** Model of hGBP1 tetramer formation. The LG domain is in red, the  $\alpha 7/11$  domain is in green and the  $\alpha 12/13$  domain is in blue. In the nucleotide-free state, hGBP1 is a monomer. For self-assembly, hGBP1 employs two different binding sites. The first binding site is located within the LG domain and this interaction is triggered by binding of GTP. Enzymatic activity of the enzyme leads to a structural shift making previously buried sites on  $\alpha 12/13$  available for interaction with another  $\alpha 12/13$  domain (as indicated by the blue arrows), leading to coiled-coil formation of two  $\alpha 12/13$  subdomains.

endogenous hGBP1. As shown in Fig. 9, after a few minutes of incubation with formaldehyde, a significant fraction of hGBP1 is covalently cross-linked to dimer and within a bigger fraction to a tetramer. This

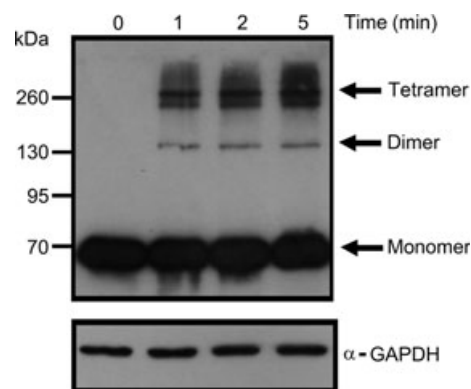


**Fig. 9.** Formaldehyde cross-linking in cells. Endogenous hGBP1 was visualized by western blotting after incubation of HUVEC cells with 1% formaldehyde solution for the time-periods indicated. Immunochemical detection of GAPDH demonstrates that equal amounts of cell lysates were loaded.

suggests that under GTP multiturnover, hGBP1 is a tetrameric protein.

## Concluding remarks

hGBP1 forms a dimer after binding of GppNHp, while GTP binding and subsequent hydrolysis leads to the formation of hGBP1 tetramers. Tetramers are also observed in the presence of GDP and aluminum fluoride. The nucleotide-dependent establishment of a contact between two LG domains is well characterized, especially by various X-ray structures. In this work we show compelling evidence that the formation of the tetramer is mediated through contacts between two  $\alpha 12/13$  domains. Moreover, this interaction is

established by the formation of a coiled-coil of two  $\alpha$ 12/13 subdomains. The contact sites employed for this become available only in the course of GTP hydrolysis, suggesting a kind of 'active' detachment of  $\alpha$ 12/13 from the rest of the protein. This interpretation is supported by the observation that the coiled-coil formation is hampered for the  $\alpha$ 7/13 fragment by weak interactions between  $\alpha$ 7/11 and  $\alpha$ 12/13 subdomains, which are not 'actively' disrupted by a GTPase-driven structural change in the LG domain as in the full-length protein. As in a living cell, the prevailing nucleotide-binding partner for hGBP1 is certainly GTP, and the hGBP1 tetramers observed after cross-linking in a cellular environment support our biochemical results. Future studies will need to establish how far nucleotide hydrolysis-driven structural changes of hGBP1 and the resulting tetramer formation play a role in the biological function.

## Experimental procedures

### Construction of hGBP1 fragments

Different constructs of hGBP1 were generated by employing standard PCR protocols and using the plasmid pQE9 containing hGBP1 as a template. Oligonucleotide primers were used that contained *Bam*HI and *Sal*I restriction sites. For details of each construct see the Supporting Information. PCR products were digested with *Bam*HI and *Sal*I and ligated into vector pGEX 4T3 (GE-Healthcare, Munich, Germany) for bacterial expression and into vectors pGBKT7 and pGADT7 for yeast two-hybrid experiments. All constructs were verified by DNA sequencing.

### Yeast two-hybrid assays

Yeast culture, transformation and two-hybrid assays were performed according to the instructions of the yeast protocol handbook and the Matchmaker 3 manual (Clontech, Heidelberg, Germany). Details of the yeast two-hybrid procedures are provided in the online Supporting Information.

### Bacterial protein expression and purification

hGBP1 protein fragments were cloned into pGEX 4T3 (GE-Healthcare) for expression of the N-terminal glutathione *S*-transferase (GST)-tagged protein in *Escherichia coli* BL21(DE3) (Novagen, Madison, WI, USA). Further information on bacterial protein expression and purification of GST-tagged proteins in *E. coli* are available in the online Supporting Information. Full-length hGBP1 was expressed from pQE9 (Qiagen, Hilden, Germany) with an N-terminal His<sub>6</sub>-tag, as described previously [20].

### CD analysis

CD spectra were recorded in buffer containing 10 mM potassium phosphate, pH 7.5, from 250 to 190 nm using a JascoJ-815 spectropolarimeter (Jasco, Gross-Umstadt, Germany). hGBP1 constructs were analyzed at concentrations from 0.09 to 100  $\mu$ M in quartz cuvettes (Hellma, Müllheim, Germany) with a path length of 0.01–1 cm. Each sample was scanned 10 times at 25 °C. Spectra were averaged, and the buffer signal was subtracted. Data were analyzed using the DICHROWEB server [29], which determines the percentage of secondary structure elements of the protein.

### Size-exclusion chromatography

Nucleotide-dependent oligomerization was monitored by size-exclusion chromatography using a Superdex S200 gel-filtration column (GE Healthcare, Munich, Germany). Proteins at 20  $\mu$ M were pre-incubated at 4 °C for 10 min in buffer C (50 mM Tris/HCl, pH 7.9, 5 mM MgCl<sub>2</sub>, 2 mM Dithioerythritol) with 200  $\mu$ M GppNHp or GDP, respectively. The column was equilibrated with buffer C and 200  $\mu$ M of the corresponding nucleotide. Additionally, for GDP and aluminium fluoride measurements, 10 mM NaF and 300  $\mu$ M AlCl<sub>3</sub> were added to the buffer. The observed elution volumes were compared with the standard proteins (Gel Filtration Markers Kit; Sigma Aldrich) that were used to calibrate the column.

### Chemical cross-linking of hGBP1 fragments

Chemical cross-linking of protein fragments was carried out using 10 mM EDC (a zero-length cross-linking agent) in the presence of 20 mM NHS in 100 mM Mes buffer at pH 6.5, or 25 mM DMS in 200 mM triethanolamine buffer, pH 7, which establishes an 11-Å linker between the lysine residues of the two proteins. Aliquots were taken at various time-points, quenched with  $\beta$ -mercaptoethanol (25 mM) or glycine for EDC and DMS, respectively, and analysed by SDS/PAGE.

### Cell culture

Primary HUVECs were purchased from PromoCell (Heidelberg, Germany) and were maintained in the corresponding endothelial cell growth medium (ECGM; PromoCell), supplemented with 2% fetal bovine serum, at 37 °C in a humidified atmosphere of 5% CO<sub>2</sub>. Before the experiment, culture dishes (Nunc, Wiesbaden, Germany) were coated for at least 2 h with 1.5% bovine skin gelatin, type B (Sigma-Aldrich, Taufkirchen, Germany) in NaCl/P<sub>i</sub> (Biochrom AG, Berlin, Germany). For stimulation with recombinant IFN- $\gamma$  (Roche, Mannheim, Germany), cells were seeded in gelatin-coated 10-cm dishes, incubated overnight in ECGM supplemented with 0.5% fetal bovine

serum and subsequently treated with  $100 \text{ U}\cdot\text{mL}^{-1}$  of recombinant IFN- $\gamma$  in the same medium for 24 h.

### Formaldehyde cross-linking in cells

Confluent, IFN- $\gamma$ -stimulated HUVECs were cross-linked for 1, 2, 5 and 10 min at room temperature by addition of a formaldehyde solution to the cell-culture medium (final concentration: 1% formaldehyde, 0.01 mM NaCl, 0.1 mM EDTA and 5 mM Hepes). Glycine (125 mM) was added to quench the reaction. Cells were subsequently washed twice with cold  $1\times$  NaCl/P<sub>i</sub>, harvested with IP-lysis buffer [20 mM Tris, 150 mM NaCl, 1% Igepal, 5 mM MgCl<sub>2</sub> supplemented with 1 tablet of protease inhibitor mix (Roche Applied Science, Mannheim, Germany) per 10 ml IP lysis buffer and lysed by sonication.

### Western blot

The protein concentration was determined using the DC assay (Bio-Rad, Munich, Germany). Western blotting from 10- $\mu\text{g}$  cell lysates was performed as previously described [8]. A monoclonal rat anti-human GBP1 IgG<sub>1</sub> (clone 1B1, 1:500 dilution [34]) and monoclonal mouse anti-human IgG<sub>1</sub> directed against glyceraldehyde-3-phosphate dehydrogenase (GAPDH, 1:50 000 dilution; Millipore, Billerica, MA, USA) were used as primary antibodies. Detection of primary antibodies was performed using an anti-rat or anti-mouse purified rabbit antiserum conjugated with horseradish peroxidase (both 1:5000 dilutions; Dako, Hamburg, Germany) and the enzymatic reaction was detected using enhanced chemiluminescence (ECL) reagents (Thermo Scientific, Roskilde, Denmark).

### Acknowledgements

This work was supported by the Deutsche Forschungsgemeinschaft (DFG, HE 2679/3-1 to C.H.; STU 317/2-1 to M.S.). E.N. was supported by the ELAN-Program of the University of Erlangen-Nuremberg. N.O. was supported by the graduate school of the University of Erlangen-Nuremberg.

### References

- 1 Praefcke GJ & McMahon HT (2004) The dynamin superfamily: universal membrane tubulation and fission molecules? *Nat Rev Mol Cell Biol* **5**, 133–147.
- 2 Mears JA, Ray P & Hinshaw JE (2007) A corkscrew model for dynamin constriction. *Structure* **15**, 1190–1202.
- 3 Anderson SL, Carton JM, Lou J, Xing L & Rubin BY (1999) Interferon-induced guanylate binding protein-1 (GBP-1) mediates an antiviral effect against vesicular stomatitis virus and encephalomyocarditis virus. *Virology* **256**, 8–14.
- 4 Itsui Y, Sakamoto N, Kakinuma S, Nakagawa M, Sekine-Osajima Y, Tasaka-Fujita M, Nishimura-Sakurai Y, Suda G, Karakama Y, Mishima K *et al.* (2009) Antiviral effects of the interferon-induced protein guanylate binding protein 1 and its interaction with the hepatitis C virus NS5B protein. *Hepatology* **50**, 1727–1737.
- 5 Naschberger E, Lubeseder-Martellato C, Meyer N, Gessner R, Kremmer E, Gessner A & Sturzl M (2006) Human guanylate binding protein-1 is a secreted GTPase present in increased concentrations in the cerebrospinal fluid of patients with bacterial meningitis. *Am J Pathol* **169**, 1088–1099.
- 6 Tietzel I, El-Haibi C & Carabeo RA (2009) Human guanylate binding proteins potentiate the anti-chlamydia effects of interferon-gamma. *PLoS One* **4**, e6499.
- 7 Guenzi E, Topolt K, Lubeseder-Martellato C, Jorg A, Naschberger E, Benelli R, Albini A & Sturzl M (2003) The guanylate binding protein-1 GTPase controls the invasive and angiogenic capability of endothelial cells through inhibition of MMP-1 expression. *EMBO J* **22**, 3772–3782.
- 8 Weinlander K, Naschberger E, Lehmann MH, Tripal P, Paster W, Stockinger H, Hohenadl C & Sturzl M (2008) Guanylate binding protein-1 inhibits spreading and migration of endothelial cells through induction of integrin alpha4 expression. *FASEB J* **22**, 4168–4178.
- 9 Naschberger E, Croner RS, Merkel S, Dimmler A, Tripal P, Amann KU, Kremmer E, Brueckl WM, Papadopoulos T, Hohenadl C *et al.* (2008) Angiostatic immune reaction in colorectal carcinoma: impact on survival and perspectives for antiangiogenic therapy. *Int J Cancer* **123**, 2120–2129.
- 10 Li M, Mukasa A, Inda MM, Zhang J, Chin L, Cavenee W & Furnari F (2011) Guanylate binding protein 1 is a novel effector of EGFR-driven invasion in glioblastoma. *J Exp Med* **208**, 2657–2673.
- 11 Yu CJ, Chang KP, Chang YJ, Hsu CW, Liang Y, Yu JS, Chi LM, Chang YS & Wu CC (2011) Identification of Guanylate-Binding Protein 1 as a Potential Oral Cancer Marker Involved in Cell Invasion Using Omics-Based Analysis. *J Proteome Res*, **10**, 3778–3788.
- 12 Lipnik K, Naschberger E, Gonin-Laurent N, Kodajova P, Petznek H, Rungaldier S, Astigiano S, Ferrini S, Stürzl M & Hohenadl C (2010) Interferon gamma-induced human guanylate binding protein 1 inhibits mammary tumor growth in mice. *Mol Med* **16**, 177–187.
- 13 Desarnaud F, Geck P, Parkin C, Carpinito G & Makarovskiy AN (2011) Gene expression profiling of the androgen independent prostate cancer cells demonstrates complex mechanisms mediating resistance to docetaxel. *Cancer Biol Ther* **11**, 204–212.
- 14 Duan Z, Foster R, Brakora KA, Yusuf RZ & Seiden MV (2006) GBP1 overexpression is associated with a

- paclitaxel resistance phenotype. *Cancer Chemother Pharmacol* **57**, 25–33.
- 15 Schwemmler M & Staeheli P (1994) The interferon-induced 67-kDa guanylate-binding protein (hGBP1) is a GTPase that converts GTP to GMP. *J Biol Chem* **269**, 11299–11305.
- 16 Ghosh A, Praefcke GJ, Renault L, Wittinghofer A & Herrmann C (2006) How guanylate-binding proteins achieve assembly-stimulated processive cleavage of GTP to GMP. *Nature* **440**, 101–104.
- 17 Kunzelmann S, Praefcke GJ & Herrmann C (2005) Nucleotide binding and self-stimulated GTPase activity of human guanylate-binding protein 1 (hGBP1). *Methods Enzymol* **404**, 512–527.
- 18 Prakash B, Praefcke GJK, Renault L, Wittinghofer A & Herrmann C (2000) Structure of human guanylate-binding protein 1 representing a unique class of GTP-binding proteins. *Nature* **403**, 567–571.
- 19 Prakash B, Renault L, Praefcke GJK, Herrmann C & Wittinghofer A (2000) Triphosphate structure of guanylate-binding protein 1 and implications for nucleotide binding and GTPase mechanism. *EMBO J* **19**, 4555–4564.
- 20 Praefcke GJ, Geyer M, Schwemmler M, Robert KH & Herrmann C (1999) Nucleotide-binding characteristics of human guanylate-binding protein 1 (hGBP1) and identification of the third GTP-binding motif. *J Mol Biol* **292**, 321–332.
- 21 Kunzelmann S, Praefcke GJ & Herrmann C (2006) Transient kinetic investigation of GTP hydrolysis catalyzed by interferon-gamma-induced hGBP1 (human guanylate binding protein 1). *J Biol Chem* **281**, 28627–28635.
- 22 Praefcke GJ, Kloep S, Benschel U, Lilie H, Prakash B & Herrmann C (2004) Identification of residues in the human guanylate-binding protein 1 critical for nucleotide binding and cooperative GTP hydrolysis. *J Mol Biol* **344**, 257–269.
- 23 Vöpel T, Kunzelmann S & Herrmann C (2009) Nucleotide dependent cysteine reactivity of hGBP1 uncovers a domain movement during GTP hydrolysis. *FEBS Lett* **583**, 1923–1927.
- 24 Guenzi E, Töpolt K, Cornali E, Lubeseder-Martellato C, Jörg A, Matzen K, Zietz C, Kremmer E, Nappi F, Schwemmler M *et al.* (2001) The helical domain of GBP-1 mediates the inhibition of endothelial cell proliferation by inflammatory cytokines. *EMBO J* **20**, 5568–5577.
- 25 Britzen-Laurent N, Bauer M, Berton V, Fischer N, Syguda A, Reipschläger S, Naschberger E, Herrmann C & Stürzl M (2010) Intracellular trafficking of guanylate-binding proteins is regulated by heterodimerization in a hierarchical manner. *PLoS One* **5**, e14246.
- 26 Fields S & Song O (1989) A novel genetic system to detect protein-protein interactions. *Nature* **340**, 245–246.
- 27 Lupas A, Van Dyke M & Stock J (1991) Predicting coiled coils from protein sequences. *Science* **252**, 1162–1164.
- 28 Mason JM & Arndt KM (2004) Coiled coil domains: stability, specificity, and biological implications. *Chem-BioChem* **5**, 170–176.
- 29 Whitmore L & Wallace BA (2004) DICHROWEB, an online server for protein secondary structure analyses from circular dichroism spectroscopic data. *Nucleic Acids Res* **32**, W668–W673.
- 30 Greenfield NJ & Hitchcock-Degregori SE (1993) Conformational intermediates in the folding of a coiled-coil model peptide of the N-terminus of tropomyosin and  $\alpha$ -tropomyosin. *Protein Sci* **2**, 1263–1273.
- 31 Zhou NE, Kay CM & Hodges RS (1992) Synthetic model proteins. *J Biol Chem* **267**, 2664–2670.
- 32 Cooper TM & Woody RW (1990) The effect of conformation on the CD of interacting helices: a theoretical study of tropomyosin. *Biopolymers* **30**, 657–676.
- 33 Vöpel T, Syguda A, Britzen-Laurent N, Kunzelmann S, Lüdemann MB, Dovengerds C, Stürzl M & Herrmann C (2010) Mechanism of GTPase-activity-induced self-assembly of human guanylate binding protein 1. *J Mol Biol* **400**, 63–70.
- 34 Lubeseder-Martellato C, Guenzi E, Jörg A, Töpolt K, Naschberger E, Kremmer E, Zietz C, Tschachler E, Hutzler P, Schwemmler M *et al.* (2002) Guanylate-binding protein-1 expression is selectively induced by inflammatory cytokines and is an activation marker of endothelial cells during inflammatory diseases. *Am J Pathol* **161**, 1749–1759.

## Supporting information

The following supplementary material is available:

**Data S1.** List of primers used.

**Data S2.** Experimental procedures: bacterial protein expression and purification.

**Data S3.** Experimental procedures and results: yeast two-hybrid assays.

**Fig. S1.** Results of the yeast two-hybrid assay.

**Fig. S2.** CD spectra of the isolated helices  $\alpha$ 7/13 and FL-hGBP1.

Please note: As a service to our authors and readers, this journal provides supporting information supplied by the authors. Such materials are peer-reviewed and may be reorganized for online delivery, but are not copy-edited or typeset. Technical support issues arising from supporting information (other than missing files) should be addressed to the authors.